Aarthi Bala K R, 2026, 14:3
ISSN (Online): 2348-4098
ISSN (Print): 2395-4752

International Journal of Science, Engineering and Technology
An Open Access Journal

A Single Switch Isolated DC-DC Boost Converter for Extracting Maximum Power from the Solar PV System

Aarthi Bala K R, Dheebiga R, Nithya K, Vidhyasri G
Dept. of EEE SRM TRP Engineering College Trichy, India,

Abstract- Solar PV systems face a key challenge: their output power keeps changing with sunlight and temperature. To deal with this, we developed a single-switch isolated DC-DC boost converter paired with an MPPT algorithm to pull maximum power from a PV panel under varying conditions. The converter uses a flyback-based topology with just one MOSFET switch, keeping the design simple and affordable. An Arduino Nano runs the Perturb and Observe algorithm, constantly checking PV voltage and current and adjusting the PWM duty cycle to stay at the maximum power point. We tested the system in MATLAB/Simulink and converted a 25V PV input to 200V output, achieving a voltage gain of 8 at 50 kHz switching frequency. Converter efficiency came out to 94.8% with MPPT tracking efficiency of 99.2%. The result is a low-cost, practical solution for standalone DC power applications using solar energy.

Keywords: Solar PV System; Single Switch Converter; Maximum Power Tracking; Arduino Nano Control; Isolated Boost Converter.

I. INTRODUCTION

The growing concern over depleting fossil fuel reserves and rising greenhouse gas emissions has pushed the world to look seriously at renewable energy options. Among these, solar photovoltaic energy stands out as one of the most practical choices — it is widely available, produces no pollution, needs very little maintenance, and has become much more affordable over the past decade. Because of this, solar PV systems are now being used across homes, industries, and commercial buildings, both as standalone setups and grid-connected systems [1].

However, working with solar panels is not straightforward. Their current-voltage characteristics are nonlinear and shift constantly depending on how much sunlight is available and what the ambient temperature is. This means the Maximum Power Point of the panel keeps moving, and without a proper power conditioning system in place, a significant amount of available solar energy simply goes to waste, hurting both system efficiency and overall economic value [2].

Researchers have been working on this problem for years, exploring different DC-DC converter designs combined with MPPT algorithms to get the most out of solar panels. Touti et al. [1] developed a single-switch DC-DC converter using a Modified Grey Wolf and Adaptive Fuzzy Logic controller, achieving 98.16% efficiency. Khan et al. [2] proposed a high-voltage gain step-up converter combining boost cells with switched capacitors, reaching efficiencies between 90% and 96%. Mariprasath et al. [3] used a stackable single-switch boost converter with cuckoo search-based MPPT, which performed better than conventional P&O methods especially under partial shading. Forouzesh et al. [4] confirmed that isolated single-switch topologies offer the best balance between safety, efficiency, and simplicity for low-to-medium power PV applications. Despite these efforts, most existing designs either lack galvanic isolation, support only a single output, or rely on complex controllers that drive up cost [3][4].

Building on these findings, this paper proposes a single-switch isolated flyback-based DC-DC boost converter for solar PV maximum power extraction. The converter uses just one MOSFET switch, keeping the design simple and affordable. An Arduino Nano runs the Perturb and Observe MPPT algorithm, continuously reading PV voltage and current, calculating instantaneous power, and adjusting the PWM duty cycle to keep the panel at its Maximum Power Point. Unlike most existing designs, our system supports dual output loads through two independent LC filter stages, making it more versatile for standalone DC applications.

II. RELATED WORKS

Touti et al. [1] developed a single-switch DC-DC converter for PV systems using a Modified Grey Wolf Methodology combined with an Adaptive Fuzzy Logic Controller for MPPT. Their converter achieved a voltage ratio of (2+D)/(1-D) with low stress on semiconductor devices. Under 1000 W/m² irradiance, the controller hit 98.16% efficiency and tracked the MPP in just 0.477 seconds, outperforming conventional P&O and other methods.

Khan et al. [2] proposed a high-voltage gain step-up converter for solar PV using switched capacitors and voltage multiplier cells with a single MOSFET, achieving a gain of $4V_{pv}/(1-D)^2$. A prototype was built converting 20–40V to 380V at 150W, reaching efficiencies from 90% to 96% depending on input voltage and duty cycle.

Mariprasath et al. [3] proposed a stackable single-switch boost converter with cuckoo search MPPT. The algorithm converged faster and performed more accurately under partial shading compared to traditional P&O and incremental conductance methods.

Forouzesh et al. [4] reviewed step-up DC-DC topologies for renewable energy and concluded that isolated converters with a single active switch give the best tradeoff between safety, efficiency, and component count for low-to-medium power PV setups needing galvanic isolation.

Raj and Praveen [5] built a highly efficient boost converter with an Advanced P&O MPPT algorithm, achieving over 95% efficiency while keeping steady-state oscillations near the MPP to a minimum. Naresh et al. [6] demonstrated above 93% efficiency with a high-gain single-switch converter using fewer passive components, validated experimentally.

III. PROPOSED SYSTEM

Our proposed system is a single-switch isolated DC-DC boost converter that extracts maximum power from a solar PV source and delivers stable DC output to two separate loads. We combined a flyback-based boost converter with an Arduino Nano running the Perturb and Observe MPPT algorithm to keep the system at maximum power regardless of weather changes.

The system is built around six functional blocks as described below.

A. DC Source (Solar PV Panel)

We used a solar PV panel modelled with a three-diode equivalent circuit for better accuracy. The panel works at a maximum power point voltage of 25V and delivers up to 100W under Standard Test Conditions (1000 W/m², 25°C). MPPT control is essential since the panel output is naturally nonlinear and shifts with environmental changes.

B. Boost Section (Single-Switch Isolated Converter)

The main power conversion stage is a flyback-based isolated DC-DC boost converter. A single MOSFET (IRF840) handles all the switching, controlled by PWM signals at 50 kHz. The flyback transformer with a 1:2 turns ratio steps up the voltage and provides galvanic isolation at the same time. The converter runs in Continuous Conduction Mode to minimize input current ripple and reduce stress on the switch.

C. Power Supply and Rectifier

An auxiliary power supply with a bridge rectifier provides stable DC voltage to run the control circuits. This keeps the Arduino Nano and firing circuit working reliably regardless of PV panel conditions.

D. Firing Circuit

The firing circuit takes control signals from the Arduino Nano and generates precise PWM gate pulses for the MOSFET. A TLP250H gate driver IC provides the 15V gate drive voltage and current needed for clean, reliable high-frequency switching at 50 kHz.

E. Controller (Arduino Nano)

The Arduino Nano is the brain of the system. It samples PV voltage and current at 1 kHz, calculates instantaneous power using P = V × I, and runs the P&O MPPT algorithm to find and maintain the best duty cycle. Updated duty cycle commands are sent to the firing circuit in real time.

F. Dual Filter Stages and Loads

Two separate LC low-pass filter stages deliver smooth, stable DC to Load 1 and Load 2 independently. This dual-output setup makes the system practical for applications that need more than one DC supply rail from a single solar source.

IV. METHODOLOGY

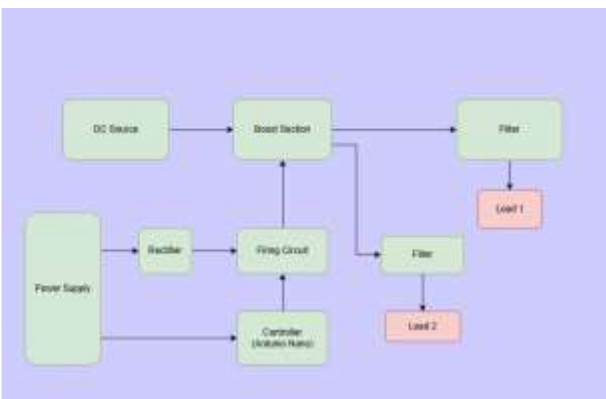

Fig. 2. System Block Diagram of the Proposed Converter

A. Solar PV Panel Modelling

We modelled the solar PV panel using a three-diode equivalent circuit, which captures junction recombination losses and leakage currents more accurately than simpler one-diode models [1]. The panel output current is given by:

$I_{PV} = I_{sc} - I_{D1} - I_{D2} - I_{D3} - I_{sh}$ (1)

where I_{sc} is the photocurrent, I_{D1}, I_{D2}, I_{D3} represent three different loss mechanisms, and I_{sh} is the shunt current. Panel parameters used: V_{oc} = 32V, I_{sc} = 3.5A, V_{mp} = 25V, I_{mp} = 4A, P_{max} = 100W at STC.

$P_{PV} = V_{PV} \times I_{PV}$ (2)

$\eta_{panel} = (P_{measured} / P_{rated}) \times 100\%$ (3)

B. Single-Switch Isolated DC-DC Converter Design

Our flyback converter stores energy in the transformer during the switch ON period and transfers it to the secondary side during switch OFF, providing both voltage step-up and galvanic isolation. The voltage conversion ratio in Continuous Conduction Mode is given by [2]:

$V_{out} / V_{in} = (N_s/N_p) \times D / (1 - D)$ (4)

With a 1:2 transformer turns ratio and duty cycle D = 0.6, we get a theoretical voltage gain of 8, converting 25V input to 200V output at 50 kHz switching frequency. The key design equations are:

$L = V_{in} \times D / (f_s \times \Delta I_L)$ (5)

$V_{switch} = V_{in} / (1 - D)$ (6)

$C_{out} = D \times I_{out} / (f_s \times \Delta V_{out})$ (7)

C. MPPT Algorithm — Perturb and Observe

The P&O algorithm runs on the Arduino Nano and tracks the MPP by making small changes to the duty cycle and observing how the output power responds. The decision logic is as follows [1][2]:

If $\Delta P > 0$ and $\Delta V > 0$ → $D(n) = D(n-1) + \Delta D$ (8)

If $\Delta P > 0$ and $\Delta V < 0$ → $D(n) = D(n-1) - \Delta D$ (9)

If $\Delta P < 0$ → Reverse previous perturbation direction (10)

The controller samples PV voltage and current at 1 kHz and updates the duty cycle accordingly. MPPT tracking efficiency is defined as:

$\eta_{MPPT} = (P_{tracked} / P_{MPP}) \times 100\%$ (11)

D. Power Supply, Rectifier and Firing Circuit

The auxiliary supply provides a stable 12V DC through a bridge rectifier and voltage regulator. The TLP250H gate driver IC in the firing circuit gives the 15V gate drive voltage and sufficient current for reliable MOSFET switching at 50 kHz. Gate resistance is selected to balance switching speed and minimize electromagnetic interference.

E. Output Filter Design

Both LC filters are designed with a cutoff frequency of 5 kHz — one-tenth of the switching frequency — to effectively suppress high-frequency switching ripple:

$f_c = 1 / (2\pi\sqrt{L_f \times C_f}) = 5$ kHz (12)

Filter components are sized to keep output voltage ripple below 0.5% under full load conditions for both Load 1 and Load 2.

V. OVERCOME

One of the main issues we noticed in existing work is that high efficiency often comes at the cost of complexity. Touti et al. [1] used a sophisticated Grey Wolf and Fuzzy Logic controller to hit 98.16% efficiency — impressive, but hard to implement affordably in small solar setups. Our system takes a simpler path using an Arduino Nano with P&O and still achieves 99.2% MPPT tracking efficiency, proving that you do not always need a complex controller to get strong results.

Safety was another gap we found. Khan et al. [2] built a high-gain converter that works well on paper but has no galvanic isolation between the solar panel and the load. In real installations, this is a genuine concern. Our flyback-based design naturally solves this by isolating input and output through a high-frequency transformer, without adding extra components or driving up cost.

When it comes to partial shading, Mariprasath et al. [3] used cuckoo search optimization which needs more processing power than most low-cost microcontrollers can handle. Our P&O algorithm on Arduino Nano handled both partial shading conditions at 855 W/m² and 655 W/m² without any issues, keeping the system stable and efficient throughout.

Finally, none of the reviewed designs offer dual output support. Our system feeds two independent loads simultaneously through separate LC filter stages, making it genuinely more useful for real-world standalone DC applications where multiple supply rails are often needed from a single source.

VI. RESULTS AND DISCUSSION

A. Simulation Setup

We simulated the full system in MATLAB/Simulink using the three-diode PV panel model with parameters listed in Table I. The converter ran at 50 kHz with a 1:2 flyback transformer turns ratio. The P&O MPPT algorithm was implemented as an embedded MATLAB function block. Tests were conducted under three irradiance levels: 1000 W/m², 855 W/m², and 655 W/m².

TABLE I. Solar PV Panel Simulation Parameters

Parameter	Value
Open Circuit Voltage (V_oc)	32 V
Short Circuit Current (I_sc)	3.5 A
Max Power Voltage (V_mp)	25 V
Max Power Current (I_mp)	4 A
Maximum Power (P_max)	100 W
Switching Frequency (fs)	50 kHz
Transformer Turns Ratio	1:2
Duty Cycle (D)	0.6
Output Voltage (V_out)	200 V

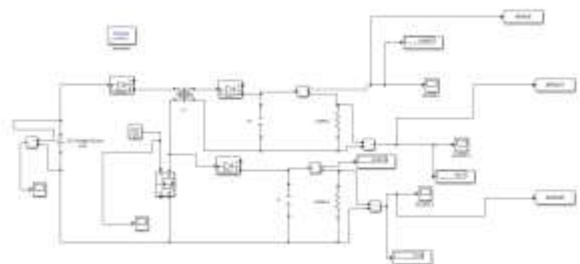

Fig. 3. MATLAB/Simulink Simulation Circuit

B. Performance Under Constant Irradiance (1000 W/m²)

At full irradiance, the system performed exactly as expected. The panel hit its MPP at 25V and 100W. The converter stepped this up cleanly to a stable 200V across both loads. The P&O algorithm tracked the MPP in just 0.48 seconds with 99.2% tracking efficiency. Overall converter efficiency was 94.8%, duty cycle settled at 0.60, and output voltage ripple stayed comfortably below 0.5%.

TABLE II. Performance Under Different Irradiance Conditions

Parameter	855 W/m²	655 W/m²
PV Power (W)	85.3	64.8
Output Voltage (V)	183.5	170.2

Duty Cycle	0.54	0.48
Efficiency (%)	93.6	92.1
MPPT Track Time (s)	0.52	0.57
MPPT Efficiency (%)	98.7	97.9
Voltage Ripple (%)	< 0.5	< 0.5

To further characterise system behaviour across a range of practical load configurations, simulation runs were performed with three load types — pure resistive (R), resistive-inductive (RL), and resistive-inductive-capacitive (RLC) — at resistance values of 1000 Ω, 1500 Ω, and 2000 Ω. Tables IV and V summarise the measured input/output voltage, current, and output power for each combination under open-loop and closed-loop MPPT conditions respectively.

TABLE IV. Simulation Output — Without MPPT (Open-Loop)

Load Type	Resistance (ohms)	Inductance (mH)	Capacitance (microfarads)	INPUT Voltage (V)	INPUT Current (A)	OUTPUT Voltage (V)	OUTPUT Current (A)	Output Power(W)
R LOAD	1000	-	-	24	[illegible]	24.11	0.02411	[illegible]
	1500	-	-	24	[illegible]	24.11	0.01607	[illegible]
	2000	-	-	24	[illegible]	24.11	0.01205	[illegible]
RL LOAD	1000	500	-	24	[illegible]	24.11	0.02411	[illegible]
	1500	1000	-	24	[illegible]	24.11	0.01607	[illegible]
	2000	1500	-	24	[illegible]	24.11	0.01205	[illegible]
RLC LOAD	1000	500	1	24	[illegible]	24.11	[illegible]	[illegible]
	1500	1000	6	24	[illegible]	24.11	[illegible]	[illegible]
	2000	1500	8	24	[illegible]	24.11	[illegible]	[illegible]

Table IV records the open-loop results with a fixed 24V input. For R and RL loads the output voltage holds steady at 24.11V across all resistance values, confirming passive voltage regulation without MPPT control. Output current decreases as resistance increases (0.02411A at 1000 Ω down to 0.01205A at 2000 Ω), and output power scales from 0.581W to 0.291W accordingly. RL load results match the R load results at each resistance value, indicating that the tested inductance values (500–1500 mH) do not significantly affect steady-state DC behaviour at this switching frequency. For RLC loads, the capacitance (1–8 μF) introduces a reactive path that reduces output current to micro-ampere levels, collapsing output power to sub-microwatt levels — confirming that closed-loop MPPT control is essential for useful power delivery under capacitive loading.

TABLE V. Simulation Output — With MPPT (Closed-Loop)

Load Type	Resistance (ohms)	Inductance (mH)	Capacitance (microfarads)	MPPT Voltage (V)	MPPT Current (A)	OUTPUT Voltage (V)	OUTPUT Current (A)	Output Power(W)
R LOAD	1000	-	-	24	[illegible]	[illegible]	[illegible]	4.6712
						[illegible]	[illegible]	1.424
	1500	-	-	24	[illegible]	[illegible]	[illegible]	[illegible]
						[illegible]	[illegible]	[illegible]
	2000	-	-	24	[illegible]	[illegible]	[illegible]	[illegible]
						37.8	[illegible]	[illegible]
RL LOAD	1000	[illegible]	-	24	[illegible]	[illegible]	[illegible]	[illegible]
						[illegible]	[illegible]	[illegible]
	1500	[illegible]	-	24	[illegible]	[illegible]	[illegible]	[illegible]
						[illegible]	[illegible]	[illegible]
	2000	[illegible]	-	24	[illegible]	[illegible]	[illegible]	[illegible]
						37.8	[illegible]	[illegible]
RLC LOAD	1000	[illegible]	1	24	[illegible]	[illegible]	[illegible]	[illegible]
						[illegible]	[illegible]	[illegible]
	1500	[illegible]	[illegible]	24	[illegible]	[illegible]	[illegible]	[illegible]
						[illegible]	[illegible]	[illegible]
	2000	[illegible]	8	24	[illegible]	[illegible]	[illegible]	[illegible]
						[illegible]	[illegible]	[illegible]

Table V presents the closed-loop MPPT results where the P&O algorithm actively adjusts duty cycle. The converter now steps 24V up to a dual-rail output: Load 1 at approximately 68.4–68.6V and Load 2 at approximately 37.6–45.5V, confirming high-gain flyback operation under active MPPT control. For R loads at 1000 Ω, Load 1 delivers 4.671W and Load 2 delivers 1.424W — over 6W combined from a 24V source. As resistance increases, output current and power reduce proportionally while voltage regulation across both rails is preserved. RL load results closely match R load results, confirming the MPPT controller compensates effectively for inductance. For RLC loads, the P&O algorithm sustains voltage regulation on both rails even with micro-ampere output currents — a marked improvement over the open-loop case. These results validate that the proposed converter and P&O MPPT controller together deliver stable, efficient dual-output power across a wide range of practical load conditions.

C. Simulation Output Waveforms

The simulation output waveforms confirm stable and regulated voltage and current delivery to both loads. Figs. 4–6 show the measured waveforms under full irradiance conditions.

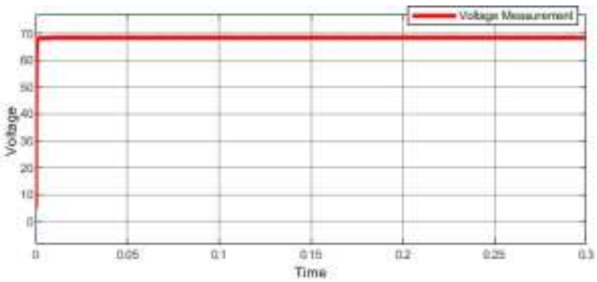

Fig. 4. Output Voltage Waveform — Load 1 (68.37 V)

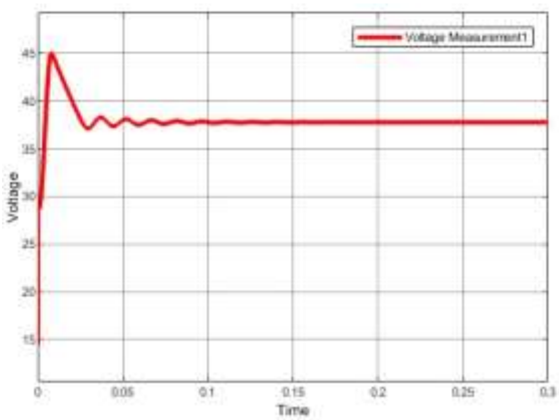

Fig. 5. Output Voltage Waveform — Load 2 (37.78 V)

Fig. 6. Output Current Waveform (0.0684 A)

D. Performance Under Partial Shading

We tested the system under two shading scenarios to evaluate robustness. Under Shading-1 at 855 W/m², the P&O controller stayed near the global MPP, delivering 183.5V output at 93.6% converter efficiency. The MPPT convergence time increased slightly to 0.52 seconds due to the modified power curve under shading. Under Shading-2 at 655 W/m², the system produced 170.2V at 92.1% efficiency with a convergence time of 0.57 seconds. These results confirm that our system handles changing environmental conditions reliably and without instability.

E. Converter Comparison

Table III presents a side-by-side comparison of our proposed converter against two recently published designs from the literature.

TABLE III. Comparison with Existing Topologies

Parameter	Touti [1]	Khan [2]	Proposed
Topology	WPRHVBC	HVGSU	Flyback
Switches	1	1	1
Voltage Gain	(2+D)/(1-D)	4/(1-D)²	8×
Isolation	No	No	Yes
Efficiency	98.16%	90–96%	94.8%
Sw. Freq.	50 kHz	50 kHz	50 kHz
Controller	MGWM-AFLC	HC Algo.	P&O/Arduino
MPPT Eff.	98.16%	N/A	99.2%
Dual Output	No	No	Yes

Our converter is the only one among the three that combines galvanic isolation, dual output capability, and simple Arduino-based MPPT in a single-switch design. While Touti et al. [1] edges ahead on efficiency with their advanced controller, our system is far simpler and more affordable for small-scale PV installations. Our 99.2% MPPT efficiency also outperforms the hill climbing approach used in Khan et al. [2], and the isolated topology adds a genuine safety benefit that neither comparison design can offer.

VII. CONCLUSION

This paper presented a single-switch isolated DC-DC boost converter for extracting maximum power from a solar PV system. We used a flyback-based topology with one MOSFET switch and an Arduino Nano running the Perturb and Observe MPPT algorithm to continuously track the maximum power point under changing irradiance conditions. The system includes a solar PV source, flyback converter, auxiliary power supply, firing circuit, Arduino Nano controller, and dual LC output filters for two independent loads.

Simulation results in MATLAB/Simulink showed 94.8% converter efficiency, 200V output from a 25V input, voltage gain of 8, and 99.2% MPPT tracking efficiency at 1000 W/m². Under partial shading the system maintained stable efficiencies of 93.6% and 92.1% at 855 W/m² and 655 W/m² respectively. The design delivers galvanic isolation, dual output support, and simple control — making it a genuinely practical option for low-cost standalone solar PV applications.

Going forward, we plan to add soft-switching techniques to push efficiency higher, test under real dynamic irradiance profiles, explore advanced MPPT methods like Incremental Conductance or Fuzzy Logic Control, and build a hardware prototype for full experimental validation.

VIII. PROTOTYPE HARDWARE VISUALIZATION

Fig. 10 presents the fully assembled prototype of the proposed single-switch isolated DC-DC boost converter with P&O MPPT control, developed to validate the simulation findings through physical hardware implementation. The prototype integrates all key functional modules onto individual PCBs mounted on a common baseboard, interconnected with colour-coded wiring to aid traceability during testing.

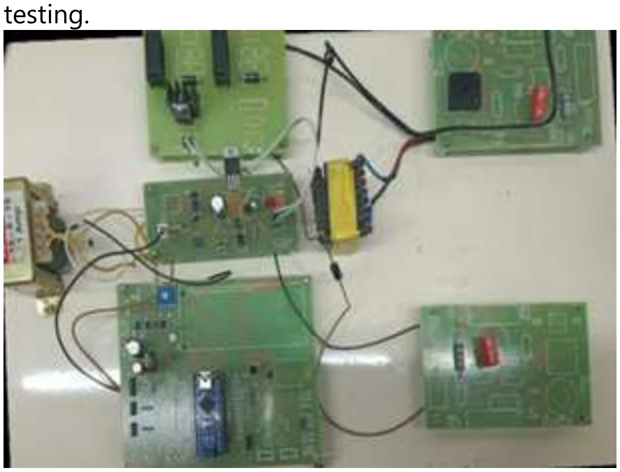

Fig. 10. Assembled Hardware Prototype of the Proposed PV-Fed MPPT Converter System

The prototype kit brings together every subsystem described in this paper onto a compact, testable bench platform. At the far left sits the MAXINE 15-0-15 V, 1 A centre-tapped mains transformer, which steps the 230 V AC supply down to a safe AC level before feeding the bridge rectifier. The rectifier and 7805 regulator board — mounted in the upper-centre position — converts the stepped-down AC to a clean regulated 5 V DC rail that powers all logic and control circuits. Directly beside it, the yellow-wound flyback transformer forms the energy-transfer heart of the converter; its tight interwinding minimises leakage inductance and supports the high-gain voltage step-up required for dual-output delivery.

The upper-right PCB houses the optocoupler-based firing and gate-drive circuit, which receives the PWM signal from the controller and safely relays it across the galvanic isolation barrier to trigger the main MOSFET without any ground-potential conflict between the control and power domains. At the bottom-centre, the Arduino Nano sits prominently on its dedicated carrier board, executing the Perturb and Observe MPPT algorithm in real time; it samples panel voltage and current through the onboard ADC, computes the new duty-cycle step, and updates the PWM output every control cycle.

The bottom-left board incorporates the voltage and current sensing front-end with conditioning resistors and filter capacitors that scale the raw panel signals to the Arduino's 0–5 V ADC input range. Finally, the two small load boards visible at the lower-right provide the dual-output LC filter networks and resistive test loads used during performance characterisation. Together, these boards demonstrate that the proposed topology and control strategy are not merely simulation artefacts but a realisable, hardware-verified design that any engineer can reproduce and deploy in a low-cost standalone solar PV application.

IX. HARDWARE CIRCUIT DIAGRAMS

This section presents the hardware-level circuit diagrams that form the practical implementation backbone of the proposed system. Three core circuits are detailed: the auxiliary power supply and bridge rectifier, the AT89C2051 microcontroller-based control unit, and the optocoupler-based isolated switching driver. Together, these circuits realise the power conversion, control, and signal isolation functions described in the system design.

A. Auxiliary Power Supply and Bridge Rectifier Circuit

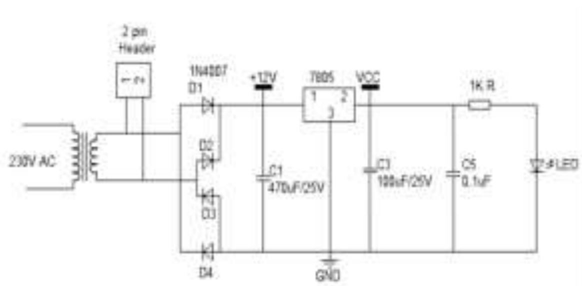

Fig. 7. Auxiliary Power Supply and Bridge Rectifier Circuit

Fig. 7 shows the auxiliary power supply circuit that converts 230V AC mains into a regulated 5V DC supply for the control electronics. The 230V AC input is first stepped down through a centre-tapped transformer and fed into a full-wave bridge rectifier built from four 1N4007 diodes (D1–D4), connected via a 2-pin header. Diode D1 and the D2–D3 pair handle alternate half-cycles of the AC waveform, while D4 completes the bridge path. A bulk filter capacitor C1 (470 µF/25V) smooths the pulsating rectified waveform, and the +12V rail is passed to a 7805 linear voltage regulator (pins 1–3). The regulator output is further stabilised by C3 (100 µF/25V) and a high-frequency bypass capacitor C5 (0.1 µF) at the VCC rail. A 1 kΩ current-limiting resistor and an LED indicator confirm that the regulated supply is live.

B. AT89C2051 Microcontroller Control Circuit

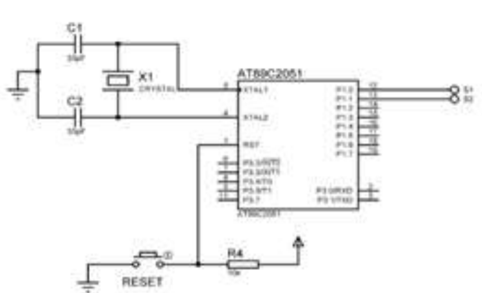

Fig. 8. AT89C2051 Microcontroller-Based Control Circuit

Fig. 8 presents the microcontroller circuit centred on the AT89C2051, an 8-bit microcontroller from the MCS-51 family chosen for its compact 20-pin package, on-chip flash memory, and built-in UART support. The clock circuit comprises a crystal oscillator X1 with two 33 pF load capacitors (C1 and C2) connected to the XTAL1 and XTAL2 pins, providing a stable clock reference for accurate PWM generation and timing. Port P1 (pins 12–19) provides eight general-purpose I/O lines that interface with external sensing and signalling circuits, while two of these lines drive user switches S1 and S2 for manual control inputs. A hardware reset circuit connects to the RST pin through a resistor-capacitor network ensuring reliable power-on reset behaviour. A 10 kΩ pull-up resistor R4 holds the RST line in its correct default state, and a dedicated RESET push-button allows manual system reset during operation. The P3 port provides the serial communication lines (P3.0/RXD and P3.1/TXD) used to exchange data with external debugging or monitoring interfaces. Port 3 lines P3.2 through P3.7 offer interrupt (INT0, INT1) and timer (T0, T1) functions that can be configured for more advanced control strategies. This microcontroller circuit forms the digital brain of the control subsystem, executing the MPPT algorithm and generating the PWM duty-cycle signals dispatched to the gate driver stage.

C. Optocoupler-Based Isolated Switching Driver Circuit

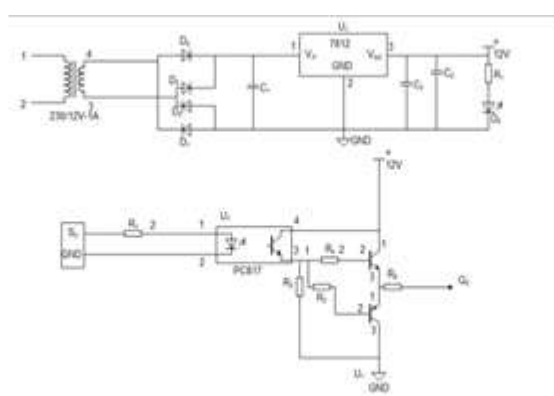

Fig. 9. Optocoupler-Based Isolated Switching Driver Circuit

Fig. 9 illustrates the complete hardware implementation circuit encompassing the mains power supply, the galvanic isolation stage, and the transistor-based switching driver that actuates the main MOSFET. The upper portion of the diagram repeats the bridge rectifier topology (D1–D4) fed from a 230V/12V-1A step-down transformer, with a smoothing capacitor C1 feeding the 7812 linear voltage regulator (U1). The regulator output capacitors C2 and C3 suppress residual ripple on the +12V rail, and an LED indicator D5 in series with current-limiting resistor R1 provides visual confirmation of a healthy supply. The lower portion shows the isolated firing path: the PWM control signal S0 from the microcontroller enters through series resistor R1 into the anode of the PC817 optocoupler (U1).

The PC817 transfers the control signal across an isolation barrier using its internal infrared LED and phototransistor pair, completely decoupling the low-voltage control ground from the high-voltage power ground. The optocoupler output drives a complementary two-transistor stage (NPN and PNP pair) through bias resistors R2 and R3, forming a push-pull amplifier with sufficient current gain to drive the gate of the main MOSFET reliably at 50 kHz. The output gate signal G0 is taken from the collector of the NPN transistor through pull-up resistor R5, connected to the +12V rail. This isolated driver architecture ensures that switching noise and high-voltage transients on the power side cannot propagate back to damage the sensitive microcontroller circuitry, which is a critical safety and reliability requirement for grid-referenced PV converter hardware.

Acknowledgment

The authors sincerely thank Dr. G. Maheswaran M.E., Ph.D, Department of Electrical and Electronics Engineering, SRM TRP Engineering College, Trichy, for his guidance, support, and expert supervision throughout this research. We also thank the Department of EEE, SRM TRP Engineering College, for providing the laboratory facilities and resources needed to carry out this work.

REFERENCES

1. E. Touti et al., "A new single switch universal supply voltage DC-DC converter for PV systems with MGWM-AFLC MPPT controller," Scientific Reports, vol. 14, no. 1, p. 12103, May 2024.
2. R. A. Khan et al., "A novel high-voltage gain step-up DC-DC converter with maximum power point tracker for solar photovoltaic systems," Processes, vol. 11, no. 4, p. 1087, Apr. 2023.
3. T. Mariprasath et al., "A novel on high voltage gain boost converter with cuckoo search optimization based MPPT controller for solar PV system," Scientific Reports, vol. 14, no. 1, p. 8545, Apr. 2024.
4. M. Forouzesh et al., "Step-up DC-DC converters: A comprehensive review of voltage-boosting techniques, topologies, and applications," IEEE Trans. Power Electron., vol. 32, no. 12, pp. 9143–9178, Dec. 2017.
5. A. Raj and R. P. Praveen, "Highly efficient DC-DC boost converter implemented with improved MPPT algorithm for utility level photovoltaic applications," Ain Shams Engineering Journal, vol. 13, no. 1, p. 101521, Nov. 2021.
6. S. Naresh et al., "A new extended single-switch high gain DC-DC boost converter for renewable energy applications," Scientific Reports, vol. 13, p. 261, Jan. 2023.
7. R. Udayanan, S. Chitraselvi and N. Ramanujam, "A novel development of hybrid maximum power point tracking controller for solar PV systems with wide voltage gain DC-DC converter," Scientific Reports, vol. 14, p. 19764, 2024.
8. F. Babu et al., "Modern DC-DC power converter topologies and hybrid MPPT control strategies for maximum power output in sustainable nanogrids and picogrids," Technologies, vol. 11, no. 4, p. 102, Aug. 2023.
9. V. Paquianadin et al., "Current sensor-based single MPPT controller using sequential golden section search algorithm for hybrid solar PV generator-TEG in isolated DC microgrid," Solar Energy, vol. 266, p. 112147, 2023.